ARTICLE

Graphene Oxide as a Promising Hole Injection Layer for MoS_2-Based Electronic Devices

Tiziana Musso,[*,†] Priyank V. Kumar,[‡] Adam S. Foster,[†] and Jeffrey C. Grossman[‡]

[†]COMP, Department of Applied Physics, Aalto University School of Science, Espoo 00076, Finland and [‡]Department of Materials Science and Engineering, Massachusetts Institute of Technology, Cambridge, Massachusetts 02139, United States

ABSTRACT The excellent physical and semiconducting properties of transition metal dichalcogenide (TMDC) monolayers make them promising materials for many applications. The TMDC monolayer MoS_2 has gained significant attention as a channel material for next-generation transistors. However, while n-type single-layer MoS_2 devices can be made with relative ease, fabrication of p-type transistors remains a challenge as the Fermi-level of elemental metals used as contacts are pinned close to the conduction band leading to large p-type Schottky barrier heights (SBH). Here, we propose the utilization of graphene oxide (GO) as an efficient hole injection layer for single-layer MoS_2-based electronic and optoelectronic devices. Using first-principles computations, we demonstrate that GO forms a p-type contact with monolayer MoS_2, and that the p-type SBH can be made smaller by increasing the oxygen concentration and the fraction of epoxy functional groups in GO. Our analysis shows that this is possible due to the high work function of GO and the relatively weak Fermi-level pinning at the MoS_2/GO interfaces compared to traditional MoS_2/metal systems (common metals are Ag, Al, Au, Ir, Pd, Pt). The combination of easy-to-fabricate and inexpensive GO with MoS_2 could be promising for the development of hybrid all-2D p-type electronic and optoelectronic devices on flexible substrates.

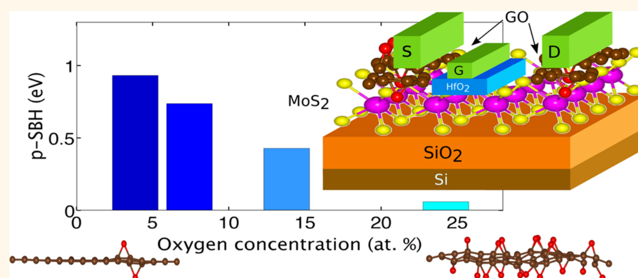

KEYWORDS: MoS_2 · graphene oxide · DFT · Schottky barrier · hole injection layer · p-type FET

Many two-dimensional (2D) materials exist in bulk form as stacks of bonded layers with weak van der Waals interlayer attraction. Thanks to their particular structure, they can be exfoliated into atomically thin monolayers that hold promise for next-generation flexible electronics and optoelectronics.[1,2] Graphene has received much attention in the past decade,[3] due in large part to exceptional electronic properties such as its ultrahigh carrier mobility. However, the absence of a band gap has limited the progress of graphene-based technologies. For example, graphene field-effect transistors (FETs) cannot be turned off effectively, and even though small band gaps have been successfully opened in graphene,[4−7] the development of devices operating at room temperature with a low stand-by power dissipation remains a challenge.[8]

On the other hand, transition-metal dichalcogenides (TMDCs) are a class of direct-band gap semiconductors that are emerging as strong candidates in next-generation nanoelectronic devices.[8−12] In the monolayer form, their lack of dangling bonds, structural stability, and mobility values comparable to Si make them optimal as channel materials in FETs.[1] In particular, FETs based on single layer MoS_2, which has a direct band gap of 1.8 eV[1,13] and mobility in the range $1-50\ cm^2\ V^{-1}\ s^{-1}$ at room temperature,[14−17] show low power dissipation,[8] efficient control over switching[9] and reduction of short-channel effects.[18,19]

However, in order to develop logic circuits based on TMDCs, it is necessary to fabricate both n- and p-type FETs. TMDC FETs based on a Schottky device architecture can transport either electrons (n-FET) or holes (p-FET) in the conducting channel, depending on whether the Schottky barrier height (SBH) is smaller relative to the conduction or the valence band, respectively.[20] While monolayer n-FETs have been widely reported, fabrication of p-FETs has been challenging.[20] This is due to the relative difficulty in designing MoS_2/metal contacts

* Address correspondence to tiziana.musso@aalto.fi.

Received for review August 12, 2014 and accepted October 27, 2014.

Published online October 27, 2014 10.1021/nn504507u

© 2014 American Chemical Society

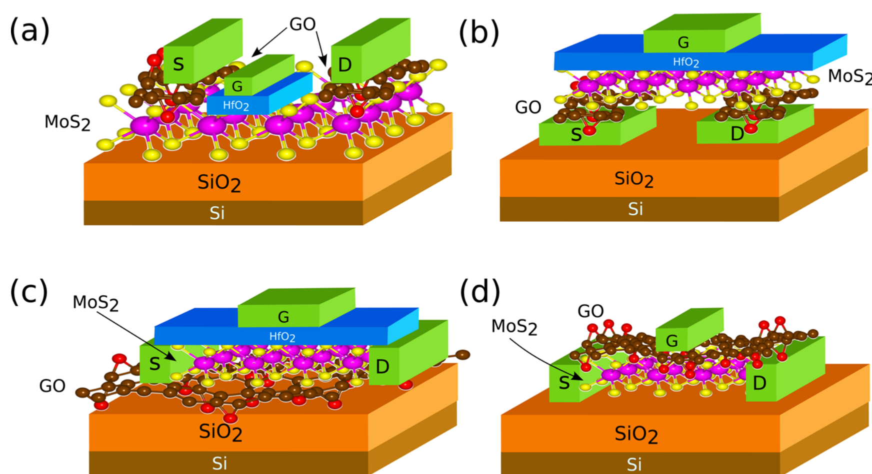

Figure 1. Possible device architectures using GO. (a) GO is used as a hole injection layer between the MoS_2 monolayer and the contacts, to obtain a p-FET. (b) An "inverted" version of the architecture shown in (a). (c) The use of MoS_2 as conductive channel and GO as substrate for tunable p-doping of the TMDC. (d) GO is directly used as a gate insulator, instead of hafnia.

with low SBH relative to the valence band. Recent density functional theory calculations for numerous metal electrodes in contact with monolayer MoS_2 show a p-type Schottky contact only in the case of platinum, while all other metal contacts lead to n-type behavior due to a Fermi level pinning mechanism at the MoS_2/metal interface.[21] As a consequence, even if high work function metals are used, the SBH to the valence band is large, producing, *de facto*, n-type devices.

In an effort to overcome this issue, Fontana et al. demonstrated the operation of p-type multilayer MoS_2 FETs through hole injection using palladium (Pd) contacts in the limit of large gate fields.[22] Recently, Chuang et al. proposed the use of substoichiometric molybdenum trioxide (MoO_x, $x < 3$), a high work function metal, as an efficient hole injection layer sandwiched between Pd and TMDC monolayers.[20] However, such inorganic hole injection layers require complex high temperature evaporation and deposition techniques in high vacuum chambers. Here, as an alternative process, we demonstrate the utilization of solution-processable graphene oxide (GO) films as promising hole injection layers for TMDC-based electronic and optoelectronic devices.

GO can be defined as a sheet of graphene with oxygen functional groups, predominantly in the form of epoxies and hydroxyls, randomly attached to its basal plane. The presence of oxygen groups disrupts the sp^2 network in graphene, thereby making it an insulator.[23] The utilization of GO in next-generation TMDC devices has many advantages. Production of GO using the widely available Hummers' method is simple and inexpensive.[23] Further, GO can be processed in solution, allowing precise control over the number of deposited GO layers, down to a monolayer.[23] Using first-principles computations, we show that GO forms a p-type contact with monolayer MoS_2, and that it is possible to tune and obtain smaller p-type SBHs by increasing the oxygen concentration and the fraction of epoxy functional groups in GO.

We present several possible device architectures (Figure 1) for fabricating FETs with GO as a hole injection layer between MoS_2 and metal contacts. One architecture is proposed in Figure 1a, where MoS_2 is used as the active channel material, and hafnia, a high-k oxide, is employed as the top-gate dielectric.[8,11] In Figure 1b, we show another possible device configuration, which is essentially "inverted", but functions similar to the one proposed in Figure 1a. Such architectures have been used recently to fabricate MoS_2 FETs with graphene contacts.[24] We point out that, experimentally, it could be easier to fabricate a device based on an "inverted" architecture, by depositing GO layers on metal contacts using lithography and etching techniques, as recently demonstrated by Roy et al.[24]

We highlight that the role of GO in MoS_2 FETs is not limited to that of obtaining p-FETs. As depicted in Figure 1c, GO can be used as a substrate to control p-type doping in MoS_2 as evidenced from our calculations. The oxygen concentration and the functional group fraction can be used as handles to tune the doping level. As an alternative, GO could be directly used as a monolayer gate insulator instead of bulk hafnia, as proposed in Figure 1d.

In integrated circuits to date,[8,25] silicon (Si) is typically used as a back-gate to tune the carrier density. It is well-known that Si, in normal stable conditions, becomes oxidized, creating a superficial layer of SiO_2. This means that, effectively, the MoS_2 monolayer is always in contact with SiO_2. The conducting properties of MoS_2 are therefore strongly influenced by the SiO_2 layer and the current polarity in an ultrathin MoS_2 monolayer deposited on SiO_2 remains unclear.[26,27] In fact, both n-type[11,13,28,29] and p-type[30] conductivities have been reported, depending on the experimental conditions. This behavior is due to the unintentional

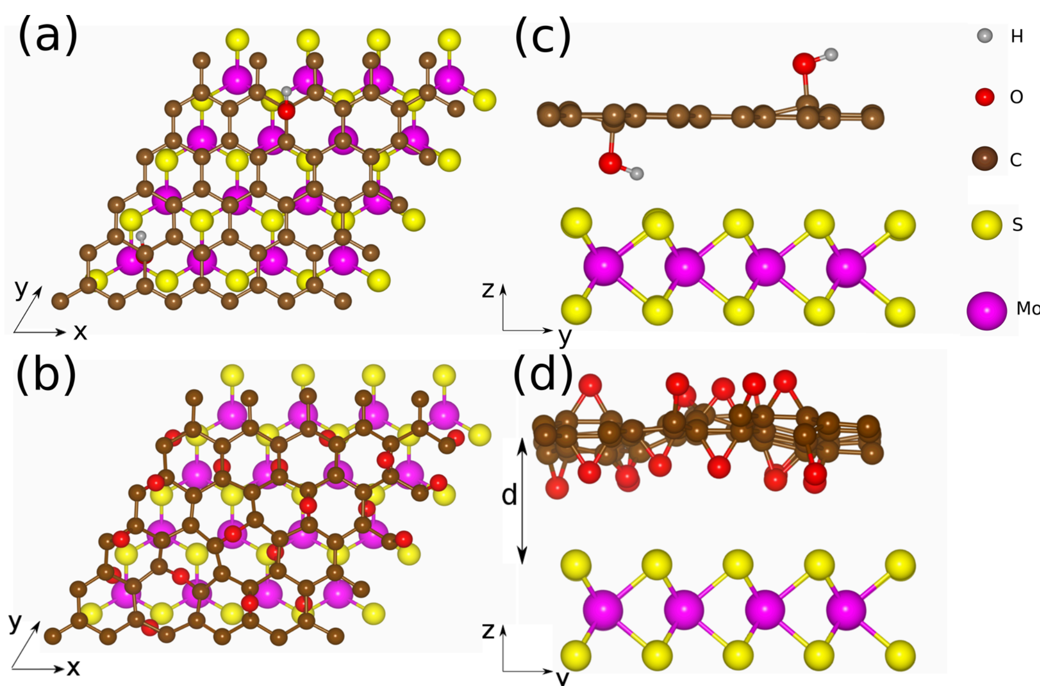

Figure 2. Example of relaxed supercells: (a,b) top view and (c,d) lateral view. In (a) and (c), the GO layer has a low oxygen concentration (4%) and is functionalized with hydroxyl groups alone. In (b) and (d), the GO layer is epoxy functionalized, with a high oxygen concentration (24%). Oxygen concentrations are given in atomic percent.

doping of SiO_2,[26] that could occur during the synthesis and sample preparation. A more reliable way to control the conductivity of the MoS_2 monolayer is to directly dope it,[27] for example, with electron irradiation[31] or sputtering techniques.[32] Other methods proposed to control the electrical and optical properties of MoS_2 rely on surface-chemistry-based approaches.[33] The use of GO as a substrate to modulate the properties of monolayer MoS_2 may be advantageous compared to the use of these more complex and expensive techniques.

In order to construct an appropriate supercell for studying MoS_2/GO interfaces, we consider an interface between a (5 × 5) layer of graphene (50 C atoms) and a (4 × 4) layer of MoS_2 (16 Mo and 32 S atoms), a combination used in previous works.[34,35] In this arrangement, the graphene lattice parameter is expanded by 3.29% to match that of MoS_2. Upon computing the electronic structure (see Supporting Information Figure S1a), we find that the band structure of strained graphene does not vary significantly from the unstrained case and retains a band gap of zero, consistent with the work of Bernardi et al.[36] Another possibility would be to strain MoS_2 while keeping graphene unstrained; this case was not considered since it led to a considerable reduction (by ~1 eV) in the band gap of MoS_2 (see Supporting Information Figure S1b). Hence, we have adopted the former configuration for all our simulations.

Regarding the stacking beween the two monolayers, different combinations have been generally adopted.[34,35,37] We have chosen the so-called TM configuration,[35] where one C atom sits exactly above a Mo atom, as illustrated in Figure 2a. Another arrangement, where a C atom sits above a S atom, has been shown to be energetically and electronically equivalent to that of the TM configuration.[34,35]

Once the graphene/MoS_2 supercell is constructed, oxygen functional groups are randomly attached above and below the graphene plane.[38,39] GO structures are obtained by relaxing the supercell without the MoS_2 monolayer first, and then the MoS_2 monolayer is introduced with an initial distance between the C plane of GO and the Mo plane of MoS_2 of 4.85 Å, which is the van der Waals distance obtained for the MoS_2/graphene case. We found that deviations from this value did not significantly change the total energy of the system for different GO structures (see Supporting Information Figure S2). This is attributed to the homogeneously distributed effects of reconstruction of the oxygen atoms bound to GO facing the interface. Our analysis of the interface energy also predicts that all the MoS_2/GO interfaces considered in this work are energetically favorable (see Supporting Information Figure S3).

GO is nonstoichiometric and has a predominance of epoxy and hydroxyl functional groups randomly attached to the graphene basal plane because of harsh conditions employed during its synthesis.[40,41] In order to account for the heterogeneity, we have constructed different interfaces, varying the epoxy to hydroxyl ratio (1:1, 2:3, 3:2, only epoxy and only hydroxyl) and the oxygen concentration (4−24%, in atom percent).[42] We further considered a statistical set of at least 10

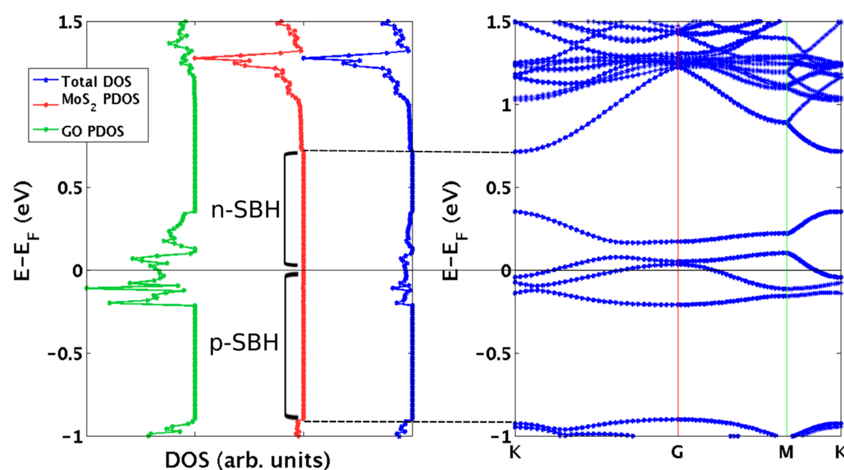

Figure 3. Example DOS plot showing the definition of n-type and p-type SBH, with the corresponding band structure.

structures for a given oxygen concentration and functional group ratio to obtain meaningful averages of the computed properties. This sampling is necessary, since the oxygen atoms in our calculations are randomly attached to the graphene plane following a uniform random distribution, thus giving GO a multitude of possible configurations.

Examples of relaxed GO/MoS_2 structures are shown in Figure 2. Upon comparing the side views in the case of GO with low (Figure 2c) and high (Figure 2d) oxygen concentrations, we note the higher graphene plane buckling in the latter case.[39] The corrugation is more emphasized when GO has a greater content of epoxy groups.

RESULTS AND DISCUSSION

We obtain a direct band gap value of 1.65 eV for monolayer MoS_2, consistent with previous DFT calculations employing the PBE functional.[21,43,44] By way of example, Figure 3 shows the density of states (DOS) and band structure plots from a single interface calculation. Note that the electronic structure of MoS_2 is minimally perturbed by the presence of GO sheets, which do not introduce defect states within the band gap of MoS_2. As expected, the electronic structure of GO presents numerous defect states within the conduction and valence band edges due to the random rearrangement of oxygen atoms on the graphene basal plane and a heterogeneous sp^2−sp^3 mixed phase.

For each hybrid structure, the DOS and the band structure have been computed to obtain a value for the MoS_2 p-type SBH. We define the energy difference between the Fermi level and the minimum of the conduction band as the n-type SBH, and similarly the p-type SBH is given by the energy difference between the valence band maximum and the Fermi energy (see Figure 3), consistent with previous DFT simulations of MoS_2/graphene contacts[36] and MoS_2/metal contacts.[21,45]

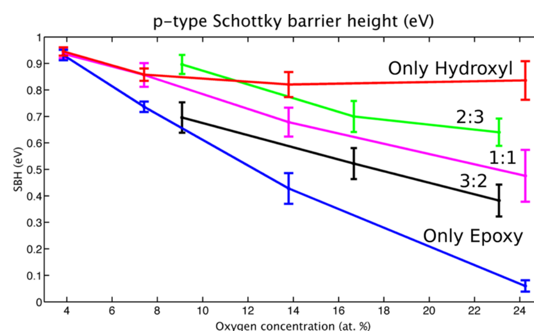

Figure 4. MoS_2 p-type SBH values as a function of the oxygen concentration in GO, using GO with different epoxy to hydroxyl ratios. The results are obtained by averaging at least 10 structures, and the error bars represent the standard error of the mean calculated for the same set of structures.

Figure 4 shows the correlation between the MoS_2 p-type SBH and the oxygen concentration in the GO monolayer, functionalized with different ratios of epoxy to hydroxyl groups. Each data point is obtained by averaging over 10 structures, and the error bars represent the standard error of the mean. The general trend is clear: p-type SBHs consistently decrease with increasing oxygen concentration for all functional group composition values considered. Furthermore, the p-type SBH can be decreased by increasing the proportion of epoxy functional groups with respect to the hydroxyl groups, an effect that grows with oxygen content. In particular, we obtained a significantly low p-type SBH value of 0.02 eV in the case of a GO sheet with ≈25% oxygen concentration, functionalized with epoxy groups alone. In addition to obtaining low SBH values, our calculations also show the possibility to tune the SBH (up to nearly 1 eV) at the MoS_2/GO interface by controlling the oxygen concentration and the relative fraction of functional groups in GO.

We next proceed to investigate the reason for the decreasing p-SBH with increasing concentration of

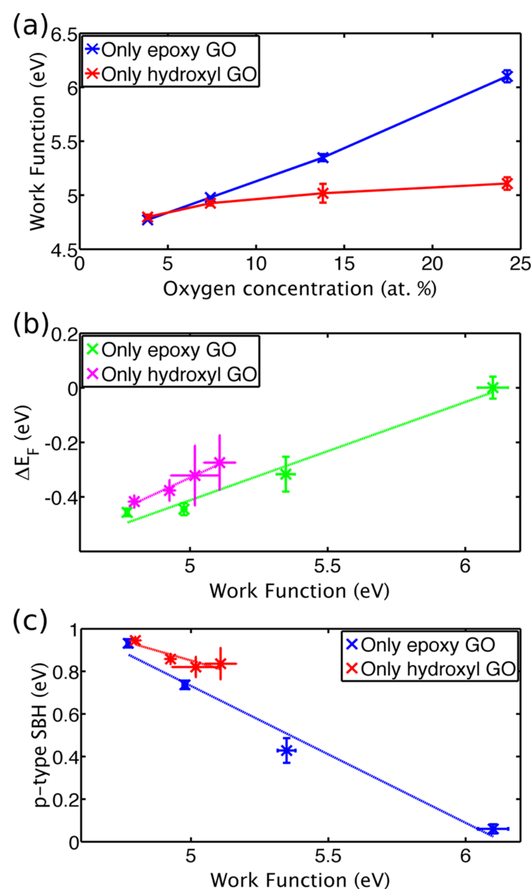

Figure 5. (a) Effect of the oxygen concentration on the work function tunability of GO, computed for GO with epoxy and hydroxyl functionalization. (b) The relative Fermi level shift of GO structures upon forming a contact with MoS_2, as a function of the corresponding work function of GO. (c) Correlation between the p-type SBH and the work function of GO. In each plot, the results are obtained by averaging over 10 structures, and the error bars represent the standard error of the mean calculated for the same set of structures. The lines in (b) and (c) are linearly interpolated.

oxygen and fraction of epoxy functional groups. It is known that the position of the Fermi-level of the adsorbate/metal system (and thus the p- and n-type SBH) can, in principle, be controlled by the work function of the metal. However, in the case of the MoS_2/metal interface, it has been demonstrated that such control is difficult to realize owing to the mechanism of Fermi-level pinning. A strong d-orbital rehybridization of Mo atoms has been observed[21] upon the formation of the interface, and the dominant contribution of these d-orbitals pins the Fermi-level close to the conduction band, leading to n-type SBH even in the case of metals with high work function (for example, Ir with a work function of 5.89 eV).[21]

In order to understand how the Fermi-level of the MoS_2/GO interfaces changes depending on the structural characteristics of GO, we have first computed the work function of hydroxyl- and epoxy-only GO (Figure 5a). As expected, the work function increases with higher oxygen concentration, although while hydroxyl functionalized GO varies by only a small amount (0.2 eV), the epoxy case changes by more than 1.2 eV, attributed to the higher electron-withdrawing ability of the epoxy groups.[46] Figure 5b shows a plot of the Fermi-level shift of GO relative to the valence band maximum of MoS_2, upon formation of the interface, as a function of the corresponding work function of GO. Linear fits give the slopes 0.36 (epoxy case) and 0.47 (hydroxyl case), values much lower than the 0.71 fitted for monolayer MoS_2 in contact with six different metals,[21] indicating that Fermi level pinning in the case of monolayer MoS_2/GO is, in comparison, weaker. We recall here that such a weak pinning of the Fermi level is necessary to achieve p-type FETs, which to date have been challenging to fabricate.

In order to shed light on the charge transfer process at the interface, we have investigated the plane-averaged electron density difference $\Delta n(z) = n_{GO|MoS_2} - n_{GO} - n_{MoS_2}$, where $n_{GO|MoS_2}$ is the total electron density of the MoS_2/GO interface system and n_{GO} and n_{MoS_2} are those of individual GO and MoS_2 structures, respectively. Figure 6 shows the charge density difference for GO with two different oxygen concentrations for the epoxy (Figure 6a,b) and hydroxyl (Figure 6c,d) functionalizations. While in GO with low oxygen concentration there is only charge depletion between MoS_2 and GO, in the high oxygen concentration case we observed charge accumulation as well. This qualitative analysis suggests that the electrons are effectively being transferred from MoS_2 toward the GO plane at higher oxygen contents (see also Supporting Information Figure S4). It should be noted that the equilibrium distance between the two monolayers depends on the oxygen content of GO. Increasing oxygen concentration progressively weakens the interlayer van der Waals bonding between MoS_2 and GO, leading to increasing interlayer separation (see Supporting Information Figure S5 for details). Moreover, our results reveal a decreased charge redistribution at the interface as well as within MoS_2, compared to that observed in MoS_2/metal systems (see Gong et al.[21]), consistent with the weaker Fermi level pinning observed here.

In addition, our PDOS plots revealed no significant gap states in contrast to some MoS_2/metal systems.[21] Such a decreased charge distribution and absence of gap states imply weaker hybridization and dipole formation at the interface. Consequently, greater variations of the p-SBH can be obtained by tuning the work function of GO (see Figure 5c).

CONCLUSION

We have used *ab initio* simulations to investigate the role of solution-processable GO as a hole injection layer for MoS_2-based devices. We demonstrate that, by increasing the oxygen concentration as well as the fraction of epoxy functional groups in GO, the p-type SBH can be decreased significantly. Our analyses show

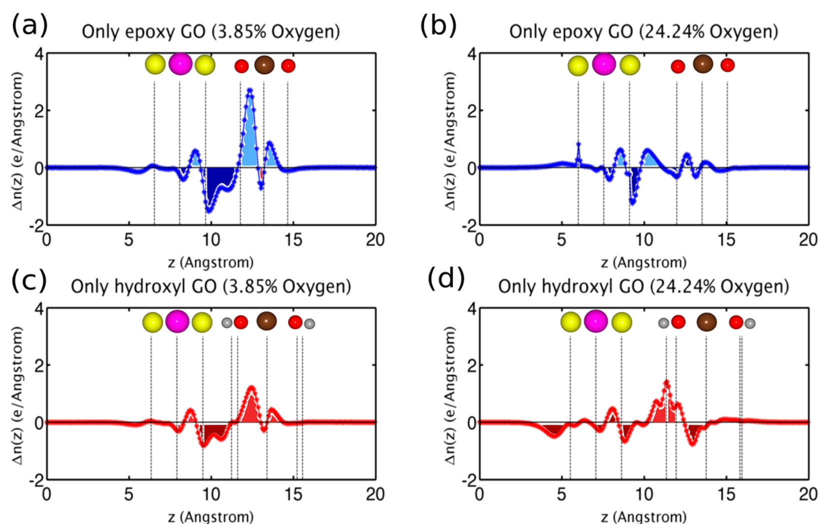

Figure 6. Plots of the plane-averaged electron density difference (Δn(z)) along the direction perpendicular to the interface of GO. (a,b) Epoxy-functionalized GO with low and high oxygen concentrations, respectively. (c,d) Corresponding plots for hydroxyl-functionalized GO. The light and dark colors indicate electron accumulation and depletion, respectively. The atomic plane positions are given at the top of each figure for reference. For the atoms legend, see Figure 2.

that the reason behind low p-type SBHs is a weak Fermi level pinning effect at the interface between GO and MoS_2, that could allow efficient p-FET device fabrication. Overall, we highlight the remarkable potential held by GO for next-generation MoS_2-based electronic and optoelectronic devices.

COMPUTATIONAL DETAILS

All calculations are performed using plane-wave density functional theory (DFT), as implemented in the VASP package.[47] We used the projector-augmented-wave method to describe the core electrons,[48,49] and the Perdew–Burke–Ernzerhof (PBE) exchange-correlation functional.[50] Van der Waals (vdW) corrections are included through Grimme's DFT-D2 method as implemented in VASP,[51,52] while the spin–orbit interactions are not accounted for here consistent with previous studies,[21,53] given that their computational cost is high (for >100 atoms in the unit cell), and their main effect being splitting of the valence band, which does not affect the computed SBH trends. A kinetic energy cutoff of 500 eV is used, and the atomic positions have been relaxed using the conjugate gradient method, until the residual atomic force on each atom is less than 0.03 eV/ Å. A vacuum region of 17 Å normal to the surface is employed to avoid interaction between the slab images. A (5 × 5 × 1) Γ-centered k-point grid is used for structural relaxations, while the k-point grid is increased to (9 × 9 × 1) to obtain the DOS and the interface band structure. The electronic properties for several cases have been computed with the hybrid HSE06 functional,[54] and good agreement with the PBE trends was observed (see Figures S6 and S7 in the Supporting Information for details). The charge-density analysis has been carried out with the grid-based Bader method.[55,56]

Conflict of Interest: The authors declare no competing financial interest.

Supporting Information Available: Figure S1: Strain effects on the DOS of graphene and MoS_2, upon building of the supercell. Figure S2: Effect of varying the distance between GO and MoS_2 monolayers. Figure S3: Interface energy as a function of the oxygen concentration in the GO layer, for only-epoxy and only-hydroxyl functionalization. Figure S4: Charge transfer at the GO/MoS_2 interface, as a function of oxygen concentration in only-epoxy and only-hydroxyl functionalization. Figure S5: Charge analysis at the MoS_2/GO interface, as a function of the interlayer distance between the two materials. Figure S6: Comparison of p-type SBH values obtained with GGA (PBE) and hybrid functional (HSE06). Figure S7: Comparison of GO gap states in the MoS_2 band gap using PBE and HSE06. Figure S8: MoS_2 band gap analysis, for GO with different concentrations of oxygen functional groups. This material is available free of charge *via* the Internet at http://pubs.acs.org/.

Acknowledgment. The authors thank the Texas Advanced Computing Center (TACC) at The University of Texas at Austin and the Finnish CSC - IT Center for Science Ltd. for providing grid resources that have contributed to the research results reported within this paper. T.M. acknowledges financial support from the Academy of Finland through its Centres of Excellence Programme (2012–2017) under Project No. 251748, MORDRED (Grant No. 261868) and The Finnish Academy of Science and Letters, Vilho, Yrjö and Kalle Väisälä Foundation. J.C.G. and P.V.K. acknowledge partial support from the Eni Solar Frontiers Program at MIT.

REFERENCES AND NOTES

1. Wang, Q. H.; Kalantar-Zadeh, K.; Kis, A.; Coleman, J. N.; Strano, M. S. Electronics and Optoelectronics of Two-Dimensional Transition Metal Dichalcogenides. *Nat. Nanotechnol.* **2012**, *7*, 699–712.
2. Novoselov, K. S.; Jiang, D.; Schedin, F.; Booth, T. J.; Khotkevich, V. V.; Morozov, S. V.; Geim, A. K. Two-Dimensional Atomic Crystals. *Proc. Natl. Acad. Sci. U. S. A.* **2005**, *102*, 10451–10453.
3. Geim, A. K.; Novoselov, K. S. The Rise of Graphene. *Nat. Mater.* **2007**, *6*, 183–191.
4. Han, M. Y.; Özyilmaz, B.; Zhang, Y.; Kim, P. Energy Band-Gap Engineering of Graphene Nanoribbons. *Phys. Rev. Lett.* **2007**, *98*, 206805.
5. Li, X.; Wang, X.; Zhang, L.; Lee, S.; Dai, H. Chemically Derived, Ultrasmooth Graphene Nanoribbon Semiconductors. *Science* **2008**, *319*, 1229–1232.
6. Zhang, Y.; Tang, T.-T.; Girit, C.; Hao, Z.; Martin, M. C.; Zettl, A.; Crommie, M. F.; Shen, Y. R.; Wang, F. Direct Observation of

a Widely Tunable Bandgap in Bilayer Graphene. *Nature* **2009**, *459*, 820–823.

7. Xia, F.; Farmer, D. B.; Lin, Y.-m.; Avouris, P. Graphene Field-Effect Transistors with High On/Off Current Ratio and Large Transport Band Gap at Room Temperature. *Nano Lett.* **2010**, *10*, 715–718.
8. Radisavljevic, B.; Whitwick, M. B.; Kis, A. Integrated Circuits and Logic Operations Based on Single-Layer MoS_2. *ACS Nano* **2011**, *5*, 9934–9938.
9. Yoon, Y.; Ganapathi, K.; Salahuddin, S. How Good Can Monolayer MoS_2 Transistors Be? *Nano Lett.* **2011**, *11*, 3768–3773.
10. Das, S.; Chen, H.-Y.; Penumatcha, A. V.; Appenzeller, J. High Performance Multilayer MoS_2 Transistors with Scandium Contacts. *Nano Lett.* **2013**, *13*, 100–105.
11. Radisavljevic, B.; Radenovic, A.; Brivio, J.; Giacometti, V.; Kis, A. Single-Layer MoS_2 Transistors. *Nat. Nanotechnol.* **2011**, *6*, 147–150.
12. Bao, W.; Cai, X.; Kim, D.; Sridhara, K.; Fuhrer, M. S. High Mobility Ambipolar MoS_2 Field-Effect Transistors: Substrate and Dielectric Effects. *Appl. Phys. Lett.* **2013**, *102*, 042104.
13. Mak, K. F.; Lee, C.; Hone, J.; Shan, J.; Heinz, T. F. Atomically Thin MoS_2: A New Direct-Gap Semiconductor. *Phys. Rev. Lett.* **2010**, *105*, 136805.
14. Radisavljevic, B.; Kis, A. Mobility Engineering and a Metal-Insulator Transition in Monolayer MoS_2. *Nat. Mater.* **2013**, *12*, 815–820.
15. Shih, C.-J.; Wang, Q. H.; Son, Y.; Jin, Z.; Blankschtein, D.; Strano, M. S. Tuning On-Off Current Ratio and Field-Effect Mobility in a MoS_2-Graphene Heterostructure via Schottky Barrier Modulation. *ACS Nano* **2014**, *8*, 5790–5798.
16. Zhu, W.; Low, T.; Lee, Y.-H.; Wang, H.; Farmer, D. B.; Kong, J.; Xia, F.; Avouris, P. Electronic Transport and Device Prospects of Monolayer Molybdenum Disulphide Grown by Chemical Vapour Deposition. *Nat. Commun.* **2014**, *5*, 3087.
17. Fuhrer, M. S.; Hone, J. Measurement of Mobility in Dual-Gated MoS_2 Transistors. *Nat. Nanotechnol.* **2013**, *8*, 146–147.
18. Schwierz, F. Nanoelectronics: Flat Transistors Get Off the Ground. *Nat. Nanotechnol.* **2011**, *6*, 135–136.
19. Schwierz, F. Graphene Transistors. *Nat. Nanotechnol.* **2010**, *5*, 487–496.
20. Chuang, S.; Battaglia, C.; Azcatl, A.; McDonnell, S.; Kang, J. S.; Yin, X.; Tosun, M.; Kapadia, R.; Fang, H.; Wallace, R. M.; *et al.* MoS_2 P-type Transistors and Diodes Enabled by High Work Function MoO_x Contacts. *Nano Lett.* **2014**, *14*, 1337–1342.
21. Gong, C.; Colombo, L.; Wallace, R. M.; Cho, K. The Unusual Mechanism of Partial Fermi Level Pinning at Metal-MoS_2 Interfaces. *Nano Lett.* **2014**, *14*, 1714–1720.
22. Fontana, M.; Deppe, T.; Boyd, A. K.; Rinzan, M.; Liu, A. Y.; Paranjape, M.; Barbara, P. Electron-Hole Transport and Photovoltaic Effect in Gated MoS_2 Schottky Junctions. *Sci. Rep.* **2013**, *3*, 1634.
23. Loh, K. P.; Bao, Q.; Eda, G.; Chhowalla, M. Graphene Oxide as a Chemically Tunable Platform for Optical Applications. *Nat. Chem.* **2010**, *2*, 1015–1024.
24. Roy, T.; Tosun, M.; Kang, J. S.; Sachid, A. B.; Desai, S. B.; Hettick, M.; Hu, C. C.; Javey, A. Field-Effect Transistors Built from All Two-Dimensional Material Components. *ACS Nano* **2014**, *8*, 6259–6264.
25. Chen, J.-R.; Odenthal, P. M.; Swartz, A. G.; Floyd, G. C.; Wen, H.; Luo, K. Y.; Kawakami, R. K. Control of Schottky Barriers in Single Layer MoS_2 Transistors with Ferromagnetic Contacts. *Nano Lett.* **2013**, *13*, 3106–3110.
26. Dolui, K.; Rungger, I.; Sanvito, S. Origin of the N-type and P-type Conductivity of MoS_2 Monolayers on a SiO_2 Substrate. *Phys. Rev. B* **2013**, *87*, 165402.
27. Dolui, K.; Rungger, I.; Das Pemmaraju, C.; Sanvito, S. Possible Doping Strategies for MoS_2 Monolayers: An *ab-initio* Study. *Phys. Rev. B* **2013**, *88*, 075420.
28. Li, H.; Lu, G.; Yin, Z.; He, Q.; Li, H.; Zhang, Q.; Zhang, H. Optical Identification of Single- and Few-Layer MoS_2 Sheets. *Small* **2012**, *8*, 682–686.
29. Lee, Y.-H.; Zhang, X.-Q.; Zhang, W.; Chang, M.-T.; Lin, C.-T.; Chang, K.-D.; Yu, Y.-C.; Wang, J. T.-W.; Chang, C.-S.; Li, L.-J.; et al. Synthesis of Large-Area MoS_2 Atomic Layers with Chemical Vapor Deposition. *Adv. Mater.* **2012**, *24*, 2320–2325.
30. Zeng, Z.; Yin, Z.; Huang, X.; Li, H.; He, Q.; Lu, G.; Boey, F.; Zhang, H. Single-Layer Semiconducting Nanosheets: High-Yield Preparation and Device Fabrication. *Angew. Chem., Int. Ed.* **2011**, *50*, 11093–11097.
31. Komsa, H.-P.; Kotakoski, J.; Kurasch, S.; Lehtinen, O.; Kaiser, U.; Krasheninnikov, A. V. Two-Dimensional Transition Metal Dichalcogenides under Electron Irradiation: Defect Production and Doping. *Phys. Rev. Lett.* **2012**, *109*, 035503.
32. Pope, L.; Jervis, T.; Nastasi, M. Effects of Laser Processing and Doping on the Lubrication and Chemical Properties of Thin MoS_2 Films. *Surf. Coat. Technol.* **1990**, *42*, 217–225.
33. Najmaei, S.; Zou, X.; Er, D.; Li, J.; Jin, Z.; Gao, W.; Zhang, Q.; Park, S.; Ge, L.; Lei, S.; *et al.* Tailoring the Physical Properties of Molybdenum Disulfide Monolayers by Control of Interfacial Chemistry. *Nano Lett.* **2014**, *14*, 1354–1361.
34. Sachs, B.; Britnell, L.; Wehling, T. O.; Eckmann, A.; Jalil, R.; Belle, B. D.; Lichtenstein, A. I.; Katsnelson, M. I.; Novoselov, K. S. Doping Mechanisms in Graphene-MoS_2 Hybrids. *Appl. Phys. Lett.* **2013**, *103*, 251607.
35. Ma, Y.; Dai, Y.; Guo, M.; Niu, C.; Huang, B. Graphene Adhesion on MoS_2 Monolayer: An *ab-initio* Study. *Nanoscale* **2011**, *3*, 3883–3887.
36. Bernardi, M.; Palummo, M.; Grossman, J. C. Extraordinary Sunlight Absorption and One Nanometer Thick Photovoltaics Using Two-Dimensional Monolayer Materials. *Nano Lett.* **2013**, *13*, 3664–3670.
37. Li, X. D.; Yu, S.; Wu, S. Q.; Wen, Y. H.; Zhou, S.; Zhu, Z. Z. Structural and Electronic Properties of Superlattice Composed of Graphene and Monolayer MoS_2. *J. Phys. Chem. C* **2013**, *117*, 15347–15353.
38. Yan, J.-A.; Xian, L.; Chou, M. Y. Structural and Electronic Properties of Oxidized Graphene. *Phys. Rev. Lett.* **2009**, *103*, 086802.
39. Nguyen, M.-T.; Erni, R.; Passerone, D. Two-Dimensional Nucleation and Growth Mechanism Explaining Graphene Oxide Structures. *Phys. Rev. B* **2012**, *86*, 115406.
40. Johari, P.; Shenoy, V. B. Modulating Optical Properties of Graphene Oxide: Role of Prominent Functional Groups. *ACS Nano* **2011**, *5*, 7640–7647.
41. Eda, G.; Chhowalla, M. Chemically Derived Graphene Oxide: Towards Large-Area Thin-Film Electronics and Optoelectronics. *Adv. Mater.* **2010**, *22*, 2392–2415.
42. Bagri, A.; Mattevi, C.; Acik, M.; Chabal, Y. J.; Chhowalla, M.; Shenoy, V. B. Structural Evolution During the Reduction of Chemically Derived Graphene Oxide. *Nat. Chem.* **2010**, 581–587.
43. Tongay, S.; Zhou, J.; Ataca, C.; Lo, K.; Matthews, T. S.; Li, J.; Grossman, J. C.; Wu, J. Thermally Driven Crossover from Indirect toward Direct Bandgap in 2D Semiconductors: $MoSe_2$ versus MoS_2. *Nano Lett.* **2012**, *12*, 5576–5580.
44. Ding, Y.; Wang, Y.; Ni, J.; Shi, L.; Shi, S.; Tang, W. First Principles Study of Structural, Vibrational and Electronic Properties of Graphene-like MX_2 (M = Mo, Nb, W, Ta; X = S, Se, Te) Monolayers. *Phys. B* **2011**, *406*, 2254–2260.
45. Gan, L.-Y.; Zhao, Y.-J.; Huang, D.; Schwingenschlögl, U. First Principles Analysis of MoS_2/Ti_2C and MoS_2/Ti_2CY_2 (Y = F and OH) All-2D Semiconductor/Metal Contacts. *Phys. Rev. B* **2013**, *87*, 245307.
46. Kumar, P. V.; Bernardi, M.; Grossman, J. C. The Impact of Functionalization on the Stability, Work Function, and Photoluminescence of Reduced Graphene Oxide. *ACS Nano* **2013**, *7*, 1638–1645.
47. Kresse, G.; Furthmüller, J. Efficient Iterative Schemes for *ab initio* Total-Energy Calculations Using a Plane-Wave Basis Set. *Phys. Rev. B* **1996**, *54*, 11169–11186.
48. Blöchl, P. E. Projector Augmented-Wave Method. *Phys. Rev. B* **1994**, *50*, 17953–17979.
49. Kresse, G.; Joubert, D. From Ultrasoft Pseudopotentials to the Projector Augmented-Wave Method. *Phys. Rev. B* **1999**, *59*, 1758–1775.

50. Perdew, J. P.; Burke, K.; Ernzerhof, M. Generalized Gradient Approximation Made Simple. *Phys. Rev. Lett.* **1996**, *77*, 3865–3868.
51. Grimme, S. Semiempirical GGA-Type Density Functional Constructed with a Long-Range Dispersion Correction. *J. Comput. Chem.* **2006**, *27*, 1787–1799.
52. Bučko, T.; Hafner, J.; Lebègue, S.; Ángyán, J. G. Improved Description of the Structure of Molecular and Layered Crystals: *Ab-initio* DFT Calculations with van der Waals Corrections. *J. Phys. Chem. A* **2010**, *114*, 11814–11824.
53. Popov, I.; Seifert, G.; Tománek, D. Designing Electrical Contacts to MoS_2 Monolayers: A Computational Study. *Phys. Rev. Lett.* **2012**, *108*, 156802.
54. Krukau, A. V.; Vydrov, O. A.; Izmaylov, A. F.; Scuseria, G. E. Influence of the Exchange Screening Parameter on the Performance of Screened Hybrid Functionals. *J. Chem. Phys.* **2006**, *125*, 224106.
55. Henkelman, G.; Arnaldsson, A.; Jónsson, H. A Fast and Robust Algorithm for Bader Decomposition of Charge Density. *Comput. Mater. Sci.* **2006**, *36*, 354–360.
56. Tang, W.; Sanville, E.; Henkelman, G. A Grid-Based Bader Analysis Algorithm Without Lattice Bias. *J. Phys.: Condens. Matter* **2009**, *21*, 084204.